RESEARCH ON DESIGN AND HYBRID SLIDING MODE CONTROL OF HIGH CLEARANCE SELF-PROPELLED SPRAYER CHASSIS AIR SUSPENSION

/

高地隙自走式喷雾机底盘空气悬架设计与混合滑模控制研究

Yu Chen[1)], Jun Chen[1)], Wei Li[2)], Shuo Zhang*[1)], Hui Xia[3)], Yahui Zhu [3)], Jiajun Wang [3)]

[1)] College of Mechanical and Electronic Engineering, Northwest A&F University, Yangling 712100, China;

[2)] College of Engineering, China Agricultural University, Beijing 100083, China;

3) Jiangsu World Agriculture Machinery Co., Ltd, Danyang 212300, China;

Tel: +86 18829225579; E-mail: zhangshuo@nwafu.edu.cn

DOI: *https://doi.org/10.35633/inmateh-61-13*

Keywords: *High clearance self-propelled sprayer, Skyhook, Groundhook, Auxiliary chamber, Sliding mode control*

ABSTRACT

According to the operation characteristics of high clearance self-propelled sprayer, an independent vertical shaft air suspension system with auxiliary chamber was designed. On the basis of the damping characteristic analysis and experiment of the air suspension with auxiliary chamber, the sprayer suspension control strategy was developed. Aiming at strong non-linearity and hysteresis for air suspension with auxiliary chamber, and when the sprayer performed road transportation and spraying operation, there was a contradiction between ride comfort and road friendliness, a hybrid sliding mode control method for sprayer chassis suspension based on skyhook reference sliding mode and ground-hook reference sliding mode was proposed. Finally, Matlab/Simulink was used to analyse the effect of the control method in different mixing coefficients. The simulation results showed that according to the requirements of different working conditions of the sprayer, by properly selecting the mixing coefficient γ value, the hybrid sliding mode control could simultaneously take into account the sprayer ride comfort and road friendliness, which was important to improve the sprayer overall performance and operating efficiency.

摘要

针对喷雾机特殊的作业特点和要求，设计了一种带附加气室的独立式立轴空气悬架系统，并在前期对带附加气室空气悬架阻尼特性分析与实验的基础上，制定了喷雾机悬架的基本控制策略。然后针对带附加气室空气悬架具有较强非线性和滞后性，且喷雾机道路转场运输和喷雾作业时，存在行驶平顺性和道路友好性之间矛盾的问题，提出了一种基于天棚参考滑模和地棚参考滑模的悬架混合滑模控制方法。最后应用 Matlab/Simulink 对不同混合系数下的控制效果进行了分析。仿真结果表明，根据喷雾机不同工况要求，合理地选择γ值，混合滑模控制可以同时兼顾喷雾机行驶平顺性和道路友好性，对提高喷雾机整机性能和作业效率具有重要意义。

INTRODUCTION

Large scale high clearance self-propelled sprayer plays a very important role in promoting food security production. However, because of the complex working conditions and unique working characteristics of the spray machine, special suspension system is needed to meet its requirements of high ground clearance, large vibration reduction stroke, convenient for four-wheel steering and wheelbase adjustment. In terms of how to reduce the dynamic load of the sprayer tire, improve the its spraying quality and ride comfort, the sprayer designers have proposed a variety of beneficial measures. For example, the designed sprayer is equipped with low-pressure, large-ground-area vacuum meridian cultivator tires, and adopts an independent chassis air suspension or hydropneumatic suspension with less unsprung mass and good nonlinearity (*Wu X H et al., 2018*). John Deere (*Carlson B C et al., 2011; Wubben T M et al., 2007*), AGCO (*Slawson J, 2013; Steffensen C et al., 2012*), HAGIE (*Schaffer J A, 2002*), AgriFac (*Blaauw D, 1999; Ehlen V and Voth R, 2011*) and other sprayer companies have applied for patents on air suspension, and their newly produced sprayers are also equipped with independent air suspension system. However, due to structural and spatial limitations, the independent air suspension system has not been equipped with damper, and only relies on the damping of tires and springs to attenuate the vibration (*Chen Y et al., 2016; 2020*). When the sprayer is running at a high speed or on the rough road conditions, the suspension vibration reduction effect will be

greatly affected. Therefore, in order to better adapt to the sprayer complex working conditions, the design of the new sprayer chassis suspension system is imminent.

In recent years, air suspension with auxiliary chamber, which uses air damping to reduce vibration, has gradually gained the attention of scholars (*Liu H and Lee J C, 2011*). Compared with traditional air suspension, air suspension with auxiliary chamber has the advantages of less heat, low manufacturing and maintenance cost (*Quaglia G et al., 2012*), better vibration reduction effect for the most sensitive frequency segment of human body (4~8Hz) (*Todkar R G, 2011*), which has been widely used in vibration reduction of commercial vehicles (*Kat C J and Els P S, 2009; Porumamilla H et al., 2008*) and rail vehicles (*Docquier N et al., 2007*). The introduction of auxiliary chamber into the sprayer's independent air suspension system can solve the problem that the suspension cannot be equipped with a damper due to structural and space constraints. Research scholars have carried out a lot of simulation and experimental research on the air suspension with auxiliary chamber structure (*Quaglia G and Sorli M, 2001; Vogel J M and Kelkar A G, 2013*), mathematical model (*Wang J, 2012*), dynamic characteristics (*Nieto A J et al., 2008; Toyofuku K et al., 1999*), control methods (*Robinson W D et al., 2012; 2013*) and so on.

Currently, there are mainly three control forms for air suspension with auxiliary chamber. One is to adjust the stiffness of the suspension by switching the auxiliary chamber with different volumes. For example, Li Z X (*2015*) applied decision control method to control the adjustable volume of the air suspension with auxiliary chamber. In this way, the suspension needed to be equipped with an adjustable shock absorber so that the suspension relative damping coefficient could be adjusted when the system stiffness changed, so as to re-matched the suspension parameters. Another method is to change the damping ratio of the system by adjusting the opening diameter of the throttle valve. Such as the research of *Porumamilla H.* (*2007*) and *Robinson W D et al.* (*2012*). The sliding mode variable structure control and linear quadratic optimal control were used to control the air spring seat suspension with auxiliary chamber. This method needed to select a suitable variable throttle valve diameter to make the system air damping have good switching performance, and to ensure that the suspension stiffness and the natural frequency changed less during the change of the system damping ratio. Another control method is to adjust the auxiliary chamber volume and the variable throttle valve diameter. For example, Jerald M V et al. (*2013*) designed a device for continuous adjustment of auxiliary chamber volume and variable throttle valve diameter. Due to the complex structure and the large number of changing parameters of the suspension system, this control method is rarely studied.

Based on this, according to the special operating characteristics and requirements of the sprayer, an independent vertical axis air suspension system with auxiliary chamber was designed. On the basis of the damping characteristic analysis and experiment of the air suspension with auxiliary chamber, the sprayer suspension control strategy was developed. Aiming at strong non-linearity and hysteresis for air suspension with auxiliary chamber, and traditional passive suspension could not take into account both road friendliness and ride comfort, a hybrid sliding mode control method for sprayer chassis suspension based on skyhook reference sliding mode and ground-hook reference sliding mode was proposed. Finally, Matlab/Simulink was used to analyse the effect of the control method in different mixing coefficients.

MATERIALS AND METHODS

Suspension structure design and vibration reduction strategy formulation

- **Suspension structure design**

The sprayer operation condition is complicated, so it not only needs to complete the transportation operation on the ordinary road, but also needs to complete the plant protection operation in the field. Two different working conditions have different requirements for suspension vibration reduction. During sprayer transportation operation, the sprayer speed is high (generally 20–40 km/h), the road conditions are good. The driver's riding comfort and the sprayer operation stability are the performance indexes that should be given priority to. Meanwhile, due to the sprayer large mass, the road friendliness should be taken into account to reduce the impact and damage to the road surface. During sprayer plant protection operation, the tire’s dynamic load should be minimized to prevent soil compaction and damage. In addition, although the sprayer speed is low (less than 20 km/h) during plant protection operation, due to the complicated road conditions in the field and the wide width of the boom, the slight tilt and vibration of the sprayer body will cause the boom to vibrate, swing and rotate, which greatly reduces Spray effect. Therefore, the sprayer ride comfort is also an important index to be considered during the its plant protection operation. In accordance with the special operating characteristics and requirements of the sprayer, based on the existing suspension

system, an independent vertical axis air suspension system with auxiliary chamber was designed, and its structural assembly wad shown in Fig.1. In the process of suspension vibration reduction, the vibration caused by the road surface is first transmitted to wheel *1*, and then transmitted to motor protection housing welding *3*, and then reaches to vertical shaft 6. Guided by the internal shaft sleeve of Beam support column welding *7*, the vibration through spring bottom support welding *21*, air spring *10*, spring top support welding *17*, guide post *19*, steering arm welding 15, positioning ring *14*, and beam *9* in order. Finally, the vibration is transmitted to the sprayer body. Air spring 10, variable throttle valve *18*, compressed air hose *11* and auxiliary chamber *12* form the suspension damping adjustment device. According to the driving conditions of the sprayer, by adjusting the opening degree of the variable throttle valve, the suspension damping is changed, and the impact load transmitted from the ground to the vehicle body is more effectively absorbed to ensure the ride comfort of the driver.

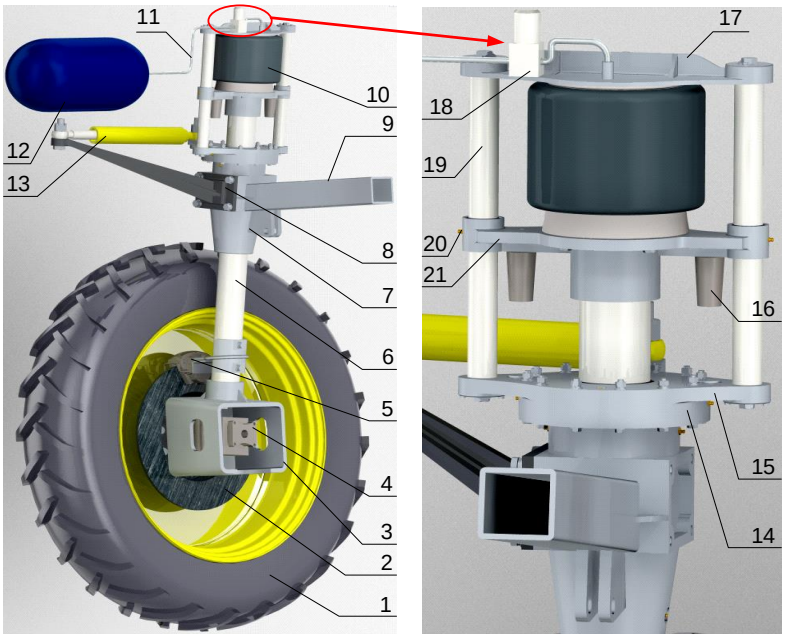

(a) Overall structure *(b) Local large map*

Fig. 1 – The structure of sprayer chassis independent vertical axis air suspension system with auxiliary chamber

1. Wheel; 2. Brake disc; 3. Motor protection housing welding; 4. Hydraulic motor; 5. Brake caliper installation welding; 6. Vertical shaft; 7. Beam support column welding; 8. Steering cylinder support arm welding; 9. Beam; 10. Air spring; 11. Compressed air hose; 12. Auxiliary chamber; 13. Steering cylinder; 14. Positioning ring; 15. Steering arm welding; 16. Rubber limit block; 17. Spring top support welding; 18. Variable throttle valve; 19. Guide post; 20. Lubrication mouth; 21. Spring bottom support welding

- **Vibration reduction strategy formulation**

By abstracting air spring *10*, compressed air hose *11*, auxiliary chamber *12* and variable throttle valve *18* in Fig.1, the vibration damping mechanism of the sprayer chassis air suspension is shown in Fig.2. Where *1* is sprung mass, *2* is air spring, *3* is variable throttle valve, *4* is auxiliary chamber, and *G* is an air mass flow rate. p_1 and p_2 are the absolute pressures of the air spring and the auxiliary chamber, respectively. V_1 and V_2 are the volumes of the air spring and the auxiliary chamber, respectively. m_b is sprung mass, x_b and w are displacements of the sprung mass and excitation, respectively. When the suspension vibrates, the air mass is exchanged between the air spring and the auxiliary chamber under the action of the excitation force. The pressure difference between the two ends of the variable throttle valve makes the air flowing through the variable throttle valve to produce damping and dissipates vibration energy.

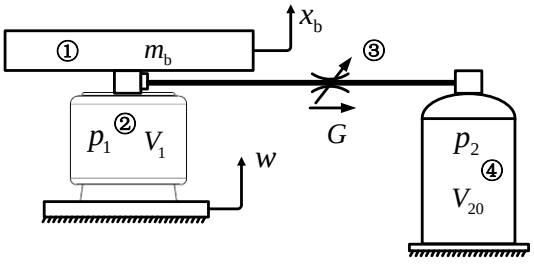

Fig. 2 - Schematic diagram of air suspension with auxiliary chamber

According to the author's previous analysis and experimental results on the damping characteristics of the sprayer chassis air suspension with auxiliary chamber (*Li W et al., 2018*), the variation relationship between the damping coefficient ζ of the air suspension with auxiliary chamber and the natural frequency ω_n and the throttle valve orifice diameter d is obtained as shown in Fig.3.

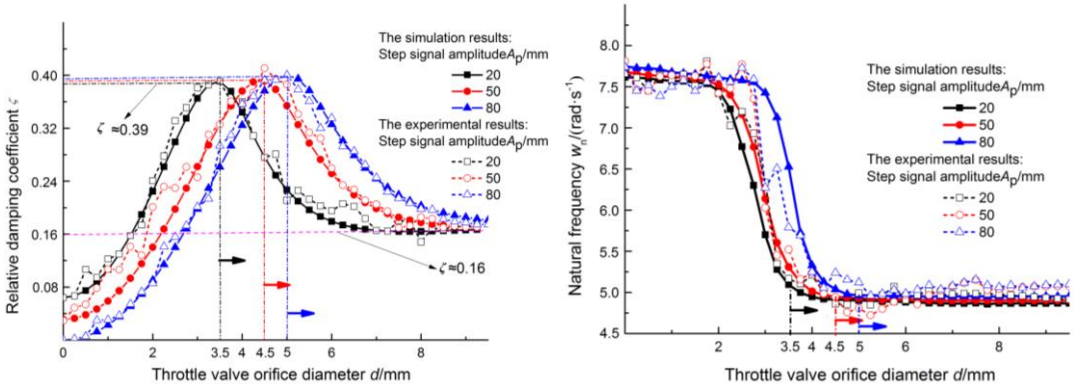

(a) Variable relationship between ζ and d *(b) Variable relationship between ω_n and d*

Fig. 3 - the variation relationship between ζ and ω_n, d

In Fig.3(a), in the area to the left of the maximum value point of relative damping coefficient, although the relative damping coefficient changes continuously with the throttle valve orifice opening, the change process is very drastic. Moreover, the spring natural frequency has a step change in this area (see Fig.3(b)), the system shows a strong nonlinearity. On the contrary, in the area to the right of the maximum value point of the relative damping coefficient, the relative damping coefficient changes continuously with the throttle valve orifice opening, and finally reaches the same value (0.16). At this point, the spring natural frequency basically remains unchanged. Therefore, when damping control is carried out on the air suspension with auxiliary chamber, the sprayer road conditions can be divided into flat road surface, uneven road surface and bad road surface. These road conditions can be simulated with step excitation amplitude of 0.02m, 0.05m and 0.08m respectively. Adjust the throttle valve opening according to different road conditions to ensure that the suspension damping ratio ζ changes between 0.39 and 0.16. Therefore, the specific control strategy of the air suspension with auxiliary chamber is as follows: when the sprayer is running on the flat road, make the throttle valve orifice opening diameter d switch between 3.5 mm and full open;When the sprayer is running on uneven road, make the throttle throttle valve orifice opening diameter d switch between 4.5mm and full open. Switch throttle valve orifice opening diameter d between 5.0 mm and full open when the sprayer is running on bad road. During the switching process of the throttle valve orifice opening, the suspension system natural frequency ω_n remains basically unchanged. This strategy will reduce the impact of changes in the parameters (such as static stiffness, natural frequency, et al.) of the air suspension system with auxiliary chamber on the system control effect.

Due to the contradiction between the ride comfort and road friendliness of the sprayer during its transportation condition and spraying condition, a trade-off must be made between the two performances. By developing appropriate suspension control strategy, the sprayer can be manually controlled or automatically controlled between ride comfort and road friendliness according to different driving conditions, so as to take into account the performance requirements of both. Meanwhile, the air suspension with auxiliary chamber has strong nonlinear and hysteresis, while the sliding mode control has high robustness to the uncertainty of model parameters and external disturbances (*Zirkohi M M et al., 2014; Assadsangabi B et al., 2009*). In order to ensure that the sprayer has good ride comfort and road friendliness under complex working conditions (*Mulla A et al., 2014*). In this paper, based on the basic control strategy of air suspension with auxiliary chamber, a hybrid control strategy combining skyhook reference sliding mode and ground-hook reference sliding mode is proposed to control the sprayer chassis air suspension.

Mathematical modeling

- **Mathematical model of suspension**

The 3D model of the sprayer independent vertical axis air suspension in Fig. 1 could be represented by the structural model of Fig. 4. The structure model in Fig. 4(a) was simplified as follows: According to the Taylor series theory, the small deviation linearization method was used to linearize the suspension stiffness k_s. The damping of air spring rubber, the damping caused by suspension element friction and other

unlabelled damping were expressed by c_s. The damping force adjusted by switching the throttle valve orifice opening between the air spring and the auxiliary chamber was represented by the suspension equivalent control force F_d. The suspension equivalent model obtained by simplification was shown in Fig. 4(b).

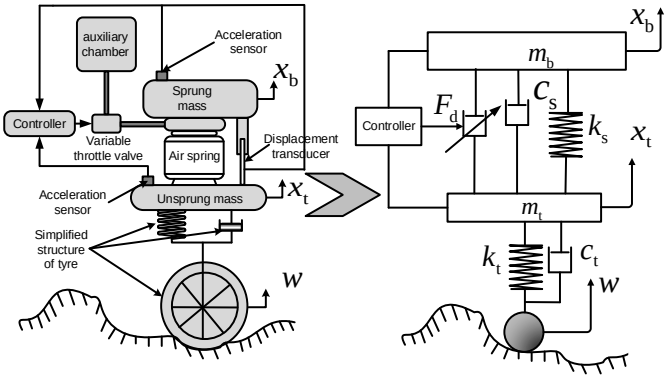

(a) Suspension structure *(b) Suspension equivalent model*

Fig. 4 - 2-DOF quarter-car suspension dynamic model

In Fig. 4: k_t – tire stiffness, N/m; c_t – tire damping, N·s/m;

m_b – sprung mass, kg; m_t – unsprung mass, kg;

x_b – sprung mass displacement, m; x_t – unsprung mass displacement, m;

w – road excitation displacement, m.

The vibration differential equation of the suspension system is:

$$\begin{cases} m_b\ddot{x}_b = -k_s(x_b - x_t) - c_s(\dot{x}_b - \dot{x}_t) - F_d \\ m_t\ddot{x}_t = k_s(x_b - x_t) + c_s(\dot{x}_b - \dot{x}_t) + F_d - k_t(x_t - w) - c_t(\dot{x}_t - \dot{w}) \\ k_s = anP_{10}A_e/(V_{10} + V_2) \end{cases} \quad (1)$$

In equation (1): α – the rate at which the volume of an air spring changes with height;

V_{10} – the volume of the air spring at the initial equilibrium position, and $V_{10}=V_2/3$;

V_2 – auxiliary chamber volume, m³;

$\ddot{x}_b$ – sprung mass acceleration, m/s²;

$\dot{x}_b$ – sprung mass speed, m/s;

$\ddot{x}_t$ – unsprung mass acceleration, m/s²;

$\dot{x}_t$ – unsprung mass speed, m/s;

$\dot{w}$ – road excitation speed, m/s.

- **Reference model**

The ideal skyhook control mainly aims at ride comfort (*Ahmadian M et al., 2004; Poussot-Vassal C et al., 2006; Priyandoko G et al., 2009*). When the dynamic load of tires deteriorates, the vehicle's handling stability becomes worse, and the large dynamic load of tires will destroy the road surface. The ideal groundhook control can reduce the dynamic load of tires by sacrificing ride comfort (*Valášek M et al., 1997; Viet L D et al., 2014*) and reduce the impact and damage of vehicles on the road surface. The ideal skyhook control model and groundhook control model are shown in Fig. 5.

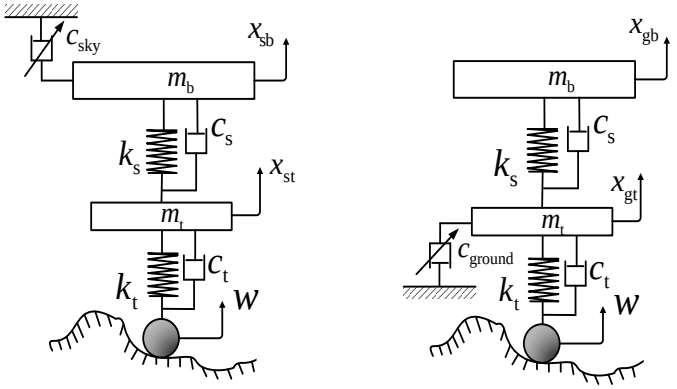

(a) The ideal skyhook control model *(b) The ideal groundhook control model*

Fig. 5 - The ideal skyhook control model and groundhook control model

The vibration differential equation of skyhook and groundhook reference control model could be expressed by equations (2) and (3). When subscript $i = s$, the equation is skyhook control.

When subscript $i = g$, the equation is groundhook control.

$$\begin{cases} m_b \ddot{x}_{sb} = -k_s\left(x_{sb} - x_{st}\right) - c_s\left(\dot{x}_{sb} - \dot{x}_{st}\right) - c_{sky}\dot{x}_{sb} \\ m_t \ddot{x}_{st} = k_s\left(x_{sb} - x_{st}\right) + c_s\left(\dot{x}_{sb} - \dot{x}_{st}\right) - k_t\left(x_{st} - w\right) - c_t\left(\dot{x}_{st} - \dot{w}\right) \end{cases} \quad (2)$$

$$\begin{cases} m_b \ddot{x}_{gb} = -k_s\left(x_{gb} - x_{gt}\right) - c_s\left(\dot{x}_{gb} - \dot{x}_{gt}\right) \\ m_t \ddot{x}_{gt} = k_s\left(x_{gb} - x_{gt}\right) + c_s\left(\dot{x}_{gb} - \dot{x}_{gt}\right) - c_t\left(\dot{x}_{gt} - \dot{w}\right) - k_t\left(x_{gt} - w\right) - c_{ground}\dot{x}_{gt} \end{cases} \quad (3)$$

In equation (2) and equation (3) : $\ddot{x}_{ib}$ – sprung mass acceleration of reference model, m/s^2;

$\dot{x}_{ib}$ – sprung mass speed of reference model, m/s;

x_{ib} – sprung mass displacement of reference model, m;

$\ddot{x}_{it}$ – unsprung mass acceleration of reference model, m/s^2;

$\dot{x}_{it}$ – unsprung mass speed of reference model, m/s;

x_{it} – unsprung mass displacement of reference model, m;

c_{sky} – damping coefficient of ideal skyhook control;

c_{groung} – damping coefficient of ideal groundhook control.

c_{sky} and c_{groung} can be expressed by the relation (4).

$$\begin{cases} c_{sky} = \begin{cases} 2\xi_{max} m_s \omega_n & \text{if } \dot{x}_{sb}\left(\dot{x}_{sb} - \dot{x}_{st}\right) \geq 0 \\ 2\xi_{min} m_s \omega_n & \text{if } \dot{x}_{sb}\left(\dot{x}_{sb} - \dot{x}_{st}\right) < 0 \end{cases} \\ c_{ground} = \begin{cases} 2\xi_{max} m_s \omega_n & \text{if } \dot{x}_{gt}\left(\dot{x}_{gb} - \dot{x}_{gt}\right) \geq 0 \\ 2\xi_{min} m_s \omega_n & \text{if } \dot{x}_{gt}\left(\dot{x}_{gb} - \dot{x}_{gt}\right) < 0 \end{cases} \end{cases} \quad (4)$$

In relation (4) : ζ_{max} – the maximum damping ratio that the suspension system can achieve when switching the variable throttle valve orifice;

ζ_{min} – the minimum damping ratio that the suspension system can achieve when switching the variable throttle valve orifice;

ω_n – Natural frequency of air suspension system with auxiliary chamber, rad/s.

Design of hybrid sliding mode controller

- **Controller design**

The air suspension with auxiliary chamber has strong nonlinearity and hysteresis. Sliding mode control is highly robust to the uncertainty of model parameters and external disturbances. In order to ensure that the sprayer has good ride comfort and road friendliness under complex working conditions, a hybrid control algorithm for the sprayer chassis suspension that combined the skyhook reference sliding mode and groundhook reference sliding mode was proposed, as shown in Fig. 6. A mixing coefficient γ was introduced into the controller to adjust the mixing degree of the two control strategies. The value of γ was [0,1]. When γ = 0, the controller was the skyhook reference sliding mode control. When γ = 1, the controller was the groundhook reference sliding mode control. The value of γ was between 0 and 1 to synthesize the characteristics of skyhook reference sliding mode control and groundhook reference sliding mode control.

The hybrid sliding mode real-time control force F_d can be expressed as:

$$F_d = \gamma F_{ssmc} + (1-\gamma) F_{gsmc} \quad (5)$$

Where: F_{ssmc} - skyhook reference sliding mode control force, N;

F_{gsmc} - groundhook reference sliding mode control force, N.

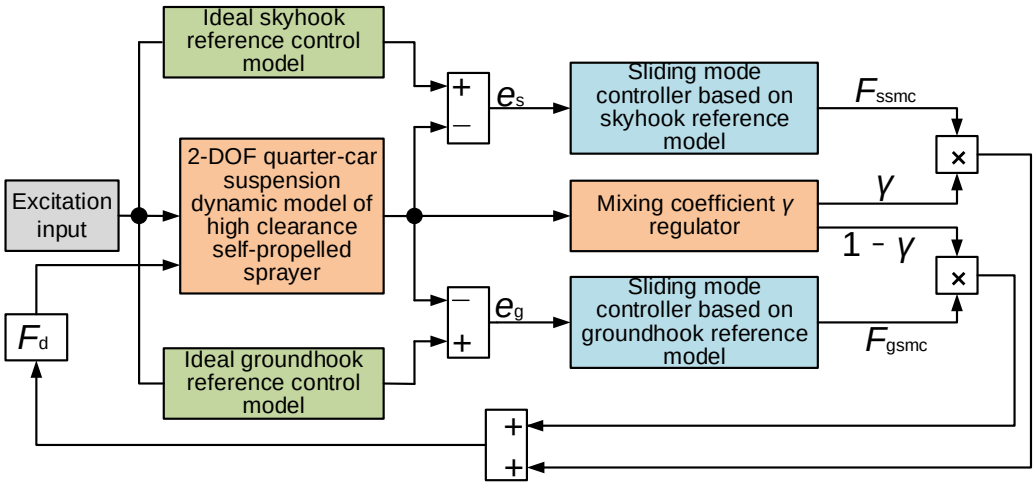

Fig. 6 - Schematic diagram of hybrid sliding mode control

- **Error dynamics model**

Because the design process of the two references sliding mode control algorithms were similar, this article took the groundhook reference sliding mode control design as an example. In order to reduce the steady-state error of the system, the integral error of unsprung mass displacement was introduced. Unsprung mass displacement integral error, unsprung mass displacement error and unsprung mass velocity error together formed the groundhook reference sliding mode control model tracking error vector $\boldsymbol{e}_g$. The error dynamics equation of groundhook reference sliding mode control was

$$\dot{\boldsymbol{e}}_g = \boldsymbol{A}_g \boldsymbol{e}_g + \boldsymbol{B}_g u_g + \boldsymbol{G}_g \boldsymbol{X} + \boldsymbol{H}_g \boldsymbol{X}_g \tag{6}$$

Where: $\boldsymbol{X}=[x_b\ x_t\ \dot{x}_b\ \dot{x}_t]$, $\boldsymbol{X}_g=[x_{gb}\ x_{gt}\ \dot{x}_{gb}\ \dot{x}_{gt}]$, $u_g=F_d$, $\boldsymbol{e}_g=[e_{g1}\ e_{g2}\ e_{g3}]^T=[\int(x_t - x_{gt})\ (x_t - x_{gt})\ (\dot{x}_t - \dot{x}_{gt})]^T$, $\dot{\boldsymbol{e}}_g=[\dot{e}_{g1}\ \dot{e}_{g2}\ \dot{e}_{g3}]^T=[(x_t - x_{gt})\ (\dot{x}_t - \dot{x}_{gt})\ (\ddot{x}_t - \ddot{x}_{gt})]^T$,

$$\boldsymbol{A}_g = \begin{bmatrix} 0 & 1 & 0 \\ 0 & 0 & 1 \\ 0 & -\frac{k_s + k_t}{m_t} & -\frac{c_s + c_t + c_{ground}}{m_t} \end{bmatrix},\ \boldsymbol{B}_g = \begin{bmatrix} 0 \\ 0 \\ \frac{1}{m_t} \end{bmatrix},\ \boldsymbol{G}_g = \begin{bmatrix} 0 & 0 & 0 & 0 \\ 0 & 0 & 0 & 0 \\ \frac{k_s}{m_t} & 0 & \frac{c_s}{m_t} & \frac{c_{ground}}{m_t} \end{bmatrix},\ \boldsymbol{H}_g = \begin{bmatrix} 0 & 0 & 0 & 0 \\ 0 & 0 & 0 & 0 \\ -\frac{k_s}{m_t} & 0 & -\frac{c_s}{m_t} & 0 \end{bmatrix}.$$

Integral sliding mode variable structure control was performed on the error dynamic system, and the integral sliding mode surface was obtained as:

$$s = \lambda_{g2} \int_0^t e_{g2} \mathrm{d}r + \lambda_{g1} e_{g2} + \dot{e}_{g2} = \boldsymbol{\Gamma} \boldsymbol{e}_g \tag{7}$$

Where: $\boldsymbol{\Gamma}$ was a coefficient matrix, and $\boldsymbol{\Gamma}$ = [λ_{g2} λ_{g1} 1], λ_{g1}, λ_{g2}> 0.

Using the pole placement method to select the coefficient matrix $\boldsymbol{\Gamma}$, the system could quickly reach the sliding mode. Assuming the system dynamic error was in the sliding mode plane, we got s = $\dot{s}$ = 0. Bring $\dot{e}_{g3}$ into $\dot{s}$ = 0, when the system entered the sliding mode, the equivalent control force F_{geq} could be gotten as:

$$F_{geq} = \left(c_s + c_t + c_{ground} - \lambda_{g1} m_t\right) e_{g3} + \left(k_s + k_t - \lambda_{g2} m_t\right) e_{g2} - c_{ground} \dot{x}_t - k_s \left(x_b - x_{gb}\right) - c_s \left(\dot{x}_b - \dot{x}_{gb}\right) \tag{8}$$

According to equation (8), the equivalent control was essentially the feedback control of partial states. F_{geq} was closely related to the system state. Due to the strong non-linearity of the air suspension with auxiliary chamber, in order to satisfy the sliding condition and enhance the robustness of the system, when the control system reached the sliding mode surface s, a discontinuous term $\varepsilon sgn(s)$ was added on F_{geq}. The actual system control F_{gsmc} was:

$$F_{gsmc} = F_{geq} + \left(-\varepsilon \operatorname{sgn}(s)\right) \qquad \varepsilon > 0 \tag{9}$$

In formula (9), ε represented the velocity of the system's motion point approaching the switching plane s=0. Reasonable selection of $\boldsymbol{\varepsilon}$ value could satisfy the system's good dynamic quality under large interference conditions.

- **System stability analysis**

Selecting Lyapunov function $V(s) = s^2/2$ and deriving it, inequality (10) could be obtained.

$$\dot{V}(s) = \frac{1}{2}\frac{d}{dt}s^2 = s\dot{s} \le -\eta|s| \tag{10}$$

In inequality (10), η>0. According to the stability theory of Lyapunov, if the inequality (11) was true, the system converged. Assuming the system was stable, we could get equation (11) by introducing equations (6), (7), and (8) into equation (10).

$$s\dot{s} = \boldsymbol{\Gamma}\left(\boldsymbol{A}_g\boldsymbol{e}_g + \boldsymbol{G}_g\boldsymbol{X} + \boldsymbol{H}_g\boldsymbol{X}_g + \boldsymbol{B}_g F_{geq}\right)s - \boldsymbol{\Gamma}\boldsymbol{B}_g\varepsilon\,\mathrm{sgn}(s)s \le -\eta|s| \tag{11}$$

Since $\varepsilon sgn(s)s = \varepsilon|s|$, and the first term of equation (11) was 0 when the system moved in the sliding mode surface, equation (11) could be rewritten as

$$-\boldsymbol{\Gamma}\boldsymbol{B}_g\varepsilon|s| \le -\eta|s| \tag{12}$$

namely

$$\varepsilon \ge \eta m_t \tag{13}$$

The inequality (13) showed that the control system was stable. By substituting (13) into (9), F_{gsmc} could be obtained as

$$F_{gsmc} = F_{geq} + (\eta m_t)\,\mathrm{sgn}(s) \tag{14}$$

In order to ensure that the variable damping force dissipated energy in real time under sliding mode control and prevented vibration deterioration, F_{gsmc} was switched by reference to groundhook logic switch control. In order to reduce the system chattering and improve the control quality, a continuous saturation function sat (s/ψ) was used instead of the discontinuous symbol function *sgn (s).* The real-time variable damping force F_{gsmc} of the groundhook reference sliding mode control was obtained as

$$F_{gsmc} = \begin{cases} F_{geq} - (\eta m_t)\,\mathrm{sat}(s/\psi), & \left(F_{geq} - (\eta m_t)\,\mathrm{sat}(s/\psi)\right)(\dot{x}_b - \dot{x}_t) \le 0 \\ 0, & \left(F_{geq} - (\eta m_t)\,\mathrm{sat}(s/\psi)\right)(\dot{x}_b - \dot{x}_t) > 0 \end{cases} \tag{15}$$

Where: ψ - boundary layer thickness, the value was 0.1.

Similarly, the real-time control force F_{ssmc} of the skyhook reference sliding mode was obtained as shown in equation (16).

$$F_{ssmc} = \begin{cases} F_{seq} + (\eta_s m_b)\,\mathrm{sat}(s_s/\psi_s), & \left(F_{seq} + (\eta_s m_b)\,\mathrm{sat}(s_s/\psi_s)\right)(\dot{x}_b - \dot{x}_t) \ge 0 \\ 0, & \left(F_{seq} + (\eta_s m_b)\,\mathrm{sat}(s_s/\psi_s)\right)(\dot{x}_b - \dot{x}_t) < 0 \end{cases} \tag{16}$$

In equation (16), F_{seq} was skyhook reference sliding mode equivalent control force. F_{seq} could be calculated by formula (17).

$$F_{seq} = (\lambda_{s2}m_b - k_s)(x_b - x_{sb}) + (\lambda_{s1}m_b - c_{sky} - c_s)(\dot{x}_b - \dot{x}_{sb}) + c_{sky}\dot{x}_b + k_s(x_t - x_{st}) + c_s(\dot{x}_t - \dot{x}_{st}) \tag{17}$$

RESULTS

Matlab/Simulink was applied to establish the control system simulation model. The simulation time interval was set as 0.005s, the simulation duration was set as 100s. Applied filtering white noise to generate a typical road excitation signal (*Popp K and Schiehlen W, 2010*). The sprayer crossed the c-class road surface at a speed of 40 km/h. The low-frequency cut-off frequency of road signal was 0.1 Hz. The road roughness coefficient was $256\times10^{-6}m^3$. Other simulation parameters were set as follows: m_s = 3000 kg, m_t = 300 kg, c_s = 2400 N·m/s, k_t = 560 KN/m, c_t = 5700 N·m/s, $\lambda_{g1} = \lambda_{s1}$ = 3.96, $\lambda_{g2} = \lambda_{s2}$ = 36.08, η_s = 3, η_g = 30, ζ_{max} = 0.39, ζ_{min} = 0.16, ω_n = 6 rad/s, α = 0.0564, $V_2 = 0.0507m^3$. Sprayer body acceleration and tire dynamic load root mean square value were selected as the evaluation indexes of ride comfort and road friendliness respectively. The influence of sliding mode control on suspension performance was analysed by changing the value of mixing coefficient γ.

The simulation results were shown in Tab. 1, Fig. 7, Fig. 8 and Fig. 9. In Tab. 1, the passive suspension referred to the simulation results when the variable throttle valve was in the optimal opening and remained unchanged, and the suspension damping coefficient ζ= 0.39.

Table 1

Comparison with simulation results

Performance indicators (RMS)	Sprung mass acceleration (m·s^{-2})	Tire dynamic load (N)	S_{sky}	S_{ground}
Passive suspension	1.56444	12430.9	——	——
γ=0	1.69968	4834.4	——	0.0081
γ=0.2	1.57673	5995.3	0.1731	0.0313
γ=0.4	1.31196	7668.8	0.07109	0.0589
γ=0.6	1.14915	9459.8	0.0436	0.09542
γ=0.8	0.87060	11990.6	0.0224	0.2146
γ=1	0.58458	13060.1	0.0065	——

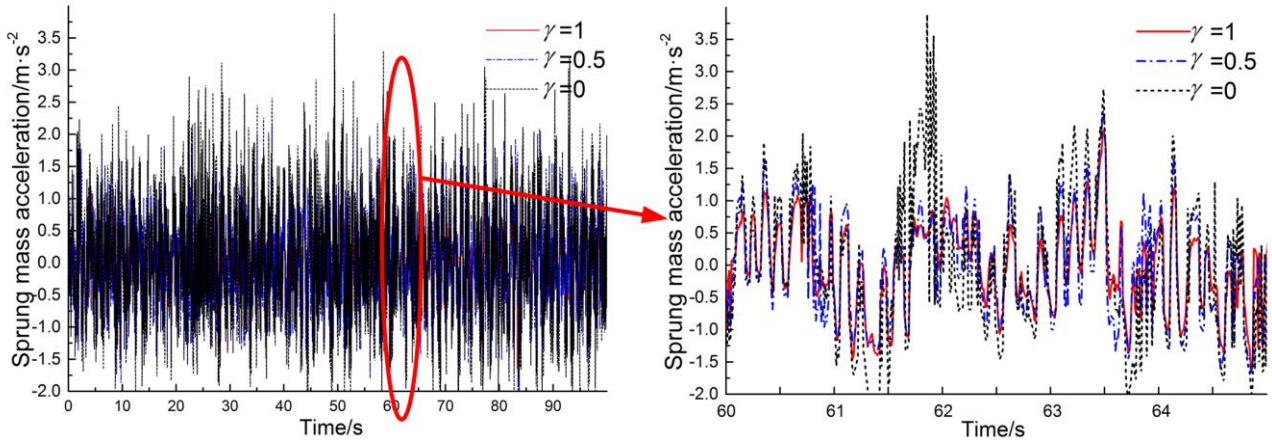

(a) Variation curve of sprung mass acceleration in time domain *(b) Local amplification*

Fig. 7 - Response curve of sprung mass acceleration in time domain

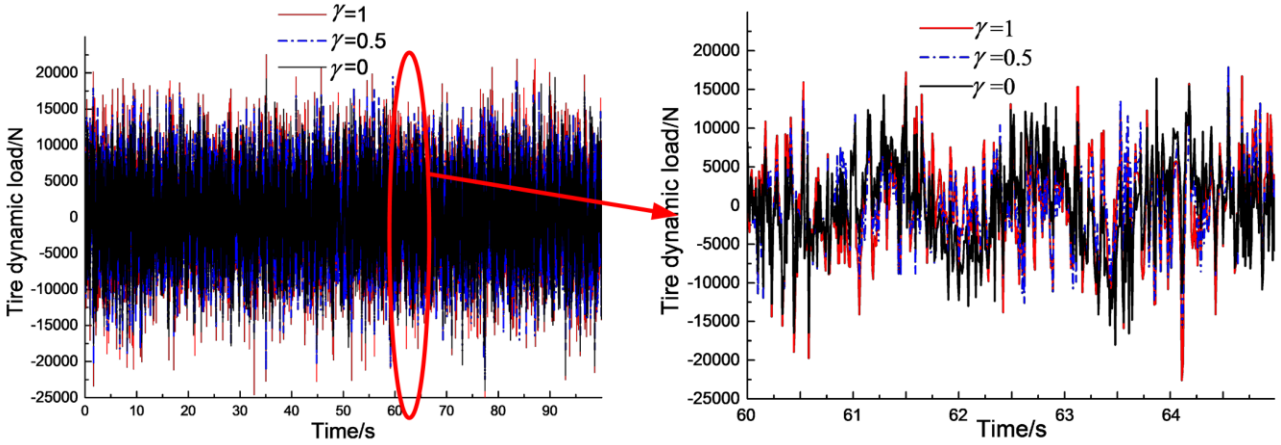

(a) Variation curve of tire dynamic load in time domain *(b) Local amplification*

Fig. 8 - Response curve of tire dynamic load in time domain

It could be seen from Tab. 1 that when the mixing coefficient γ value changed, the root mean square values of the sliding surface S_{ground} and S_{sky} were both small. It showed that the control system could track the ideal skyhook reference model and ideal groundhook reference model well. When γ =0, the hybrid sliding mode control was equivalent to the groundhook reference sliding mode control. At this time, the tire dynamic load was small and the sprayer had good road friendliness. When γ =1, the hybrid sliding mode control was equivalent to the skyhook reference sliding mode control. At this time, the sprung mass acceleration was

small and the sprayer had good ride comfort. The γ value was larger, the hybrid sliding mode control was closer to skyhook reference sliding mode control, and the sprayer ride comfort was better. The γ value was smaller, the hybrid sliding mode control was closer to groundhook reference sliding mode control, and the sprayer road friendliness was better.

When the values of γ were 0, 0.5 and 1, the corresponding responses in time and frequency domain of the sprung mass acceleration and the tire dynamic load were obtained, as shown in Fig. 7, Fig. 8 and Fig. 9. In Fig. 7, when γ =0.5, the corresponding peak - peak of sprung mass acceleration increased compared with γ =1, and decreased compared with γ =0. The sprayer ride comfort could be improved by increasing γ value. In Fig. 8, when γ value was reduced, the tire dynamic load was also reduced and the sprayer road friendliness was effectively improved.

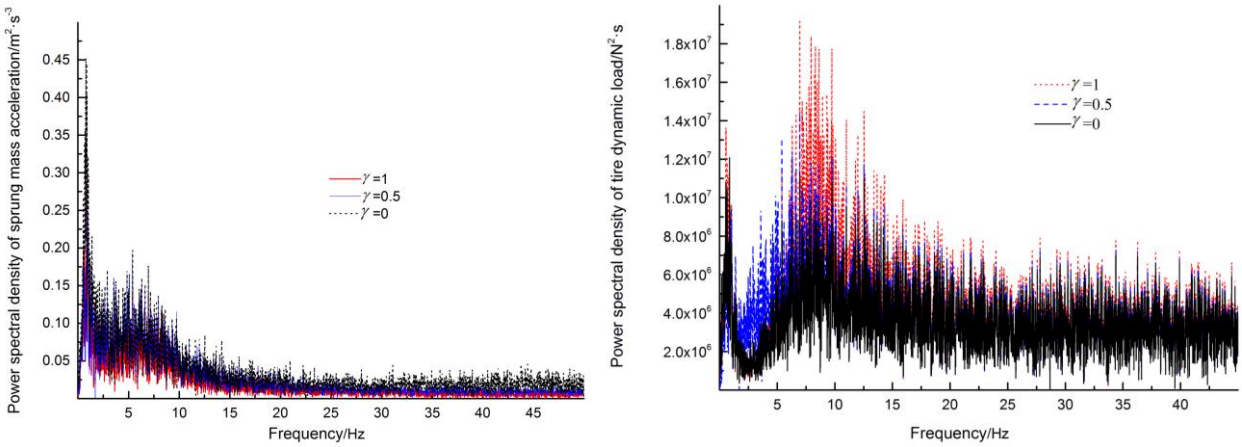

(a) Sprung mass acceleration frequency domain *(b) Tire dynamic load in frequency domain*

Fig. 9 - The curve of power spectral density

The Fig. 9 showed that in the vicinity of 1.2 Hz and 9 Hz, the sprung mass acceleration power spectrum density corresponding to γ = 0.5 was smaller than that when γ = 0 and bigger than that when γ = 1. The tire dynamic load power spectral density corresponding to γ = 0.5 was bigger than that when γ = 0, and smaller than that when γ = 1. It showed that the hybrid sliding mode control could combine the advantages of skyhook sliding mode control and groundhook sliding mode control, and had good comprehensive performance.

As could be seen from Tab. 1, Fig. 7, Fig. 8 and Fig. 9, although the hybrid sliding mode control could not achieve the effect of groundhook reference sliding mode control in terms of road friendliness, and could not achieve the effect of the skyhook reference sliding mode control in terms of ride comfort, but according to the sprayer different requirements, the mixing coefficient γ was reasonably selected, and the hybrid sliding mode control could take into account both ride comfort and road friendliness.

CONCLUSIONS

(1) According to the special operation characteristics and requirements of sprayer, an independent vertical shaft air suspension system with auxiliary chamber was designed.

(2) A damping control strategy for the sprayer suspension was presented. According to the different road surface, the variable throttle valve orifice opening was adjusted, the designed suspension system damping ratio ζ changed between 0.39 and 0.16. During the whole valve orifice being adjusted process, the system natural frequency ω_n basically remained unchanged.

(3) A hybrid sliding mode control method which combined skyhook reference sliding mode and groundhook reference sliding mode was proposed to control the sprayer suspension. When the mixing coefficient γ value was changed, the root mean square values of S_{ground} and S_{sky} were both small, the established control system could track the ideal skyhook reference model and groundhook reference model well.

ACKNOWLEDGEMENT

The authors thank the editing team of EditorBar for improving the English language fluency of our paper. The work in this paper was supported by the National Key Research and Development Program (No.2018YFD0701100-2018YFD0701102), the Key Research and Development Program of Shaanxi Province (No. 2019ZDLNY02-01) and the China Postdoctoral Science Foundation (No.2018M643744).

REFERENCES

[1] Ahmadian M, Song X, Southward S C., (2004), No-jerk skyhook control methods for semiactive suspensions, *J. Vib. Acoust*., vol.126, pp.580-584;

[2] Assadsangabi B., Eghtesad M., Daneshmand F. et al., (2009), Hybrid sliding mode control of semi-active suspension systems, *Smart Materials and Structures*, vol.18, pp.406-414.

[3] Blaauw D., (1999), *Spring-mounted spreading device*, EP, 0919124 A1;

[4] Carlson B.C., Young D.E., Baxter G.E. et al., (2011), *Suspended axle for sprayer*, US, 7938415;

[5] Chen Y., Chen S.Y., Du Y.F. et al., (2016), Damping characteristics of chassis suspension system of high clearance agricultural machinery based on friction damper(基于摩擦阻尼的高地隙农机底盘悬架减振特性), *Transactions of the CSAE*, vol.34, pp.51-57;

[6] Chen Y., Zhang S., Mao E.R. et al, (2020), Height stability control of a large sprayer body based on air suspension using the sliding mode approach, *Information Processing in Agriculture*, vol.7, pp.20-29;

[7] Docquier N., Fisette P., Jeanmart H., (2007), Multiphysics modelling of railway vehicles equipped with pneumatic suspensions, *Vehicle System Dynamics*, vol.45, pp.505-524;

[8] Ehlen V., Voth R., (2011), Suspension for self-propelled spreading machine, EP, 2388157 A1;

[9] Kat C.J., Els P.S., (2009), Interconnected air spring model, *Mathematical & Computer Modelling of Dynamical Systems*, vol.15, pp.353-370;

[10] Liu H., Lee J.C., (2011), Model development and experimental research on an air spring with auxiliary reservoir, *International Journal of Automotive Technology*, vol.12, pp.839-847;

[11] Li W., Chen Y., Zhang S. et al., (2018), Damping characteristic analysis and experiment of air suspension with auxiliary chamber, *IFAC-PapersOnLine*, vol.51, pp.166–172;

[12] Li Z.X., Ju L.Y., Jiang H. et al., (2015), Parameter optimization and control of air suspension with adjustable auxiliary chamber [J]. *Automotive Engineering*, vol.37, pp.941-945;

[13] Mulla A., Jalwadi S., Unaune D., (2014), Performance analysis of skyhook, groundhook and hybrid control strategies on semiactive suspension system, *International Journal of Current Engineering and Technology*, vol.3, pp.265-269;

[14] Nieto A.J., Morales A.L., González A. et al., (2008), An analytical model of pneumatic suspensions based on an experimental characterization, *Journal of Sound & Vibration*, vol.313, pp.290-307;

[15] Popp K., Schiehlen W., (2010), Ground vehicle dynamics, Berlin: Springer publisher;

[16] Porumamilla H., Kelkar A.G., Vogel J.M., (2008), Modeling and verification of an innovative active pneumatic vibration isolation system, *Journal of Dynamic Systems Measurement & Control*, vol.130, pp.1750-1753;

[17] Porumamilla H., (2007), *Modeling, analysis and non-linear control of a novel pneumatic semi-active vibration isolator: A concept validation study*, Ames: Iowa State University;

[18] Poussot-Vassal C., Sename O., Dugard L. et al., (2006), Optimal skyhook control for semi-active suspensions, *IFAC Proceedings Volumes*, vol.39, pp.608-613;

[19] Priyandoko G., Mailah M., Jamaluddin H., (2009), Vehicle active suspension system using skyhook adaptive neuro active force control, *Mechanical systems and signal processing*, vol.23, pp.855-868;

[20] Quaglia G., Sorli M., (2011), Air suspension dimensionless analysis and design procedure, Vehicle System Dynamics: *International Journal of Vehicle Mechanics & Mobility*, vol.35, pp.443-475;

[21] Quaglia G., Scopesi M., Franco W., (2012), A comparison between two pneumatic suspension architectures, *Vehicle System Dynamics*, vol.50, pp.509-526;

[22] Robinson W.D., Kelkar A.G., Vogel J.M., (2013), Semi-active control methodology for control of air spring-valve-accumulator system, *ASME 2013 Dynamic Systems and Control Conference*;

[23] Robinson W.D., (2012), *A pneumatic semi-active control methodology for vibration control of air spring based suspension systems*, Ames: Iowa State University;

[24] Schaffer J.A., (2002), *Steering system for variable height agricultural sprayer*, US, 6371237 B1;

[25] Schaffer J.A., (2002), *Wheel support system for agricultural sprayer*, US, 6491306 B2;
[26] Slawson J., (2013), *Independent strut suspension*, US, 8534686;
[27] Steffensen C., Michels E., Kleven J.E., (2012), *Suspension assemblies with bump steer control*, US, 8136824;
[28] Todkar R.G., (2011), Design, development and testing of an air damper to control the resonant response of a SDOF quarter-car suspension system, *Modern Mechanical Engineering*, vol.1, pp.84-92;
[29] Toyofuku K., Yamada C., Kagawa T. et al., (1999), Study on dynamic characteristic analysis of air spring with auxiliary chamber, *Jsae Review*, vol.20, pp.349-355;
[30] Valášek M., Novak M., Šika Z. et al., (1997), Extended ground-hook-new concept of semi-active control of truck's suspension, *Vehicle system dynamics*, vol.27, pp.289-303;
[31] Viet L.D., Nghi N.B., Hieu N.N. et al., (2014), On a combination of ground-hook controllers for semi-active tuned mass dampers, *Journal of Mechanical Science and Technology*, vol.28, pp.2059-2064;
[32] Vogel J.M., Kelkar A.G., (2013), *Continuously variable natural frequency and damping vibration isolation system*, US, US8490952 B1;
[33] Wang J., (2012), *Nonlinear modeling and h-infinity model reference control of pneumatic suspension system*, Ames: Iowa State University;
[34] Wubben T.M., Maiwald M.A., Carlson B.C. et al., (2007), *High clearance vehicle suspension with twin spindles for transferring steering torque*, US, 7168717 B2;
[35] Wu X.H., Qin J.H., Du Y.F. et al., (2018), Experiments of vibration control for active pneumatic suspension system in high clearance self-propelled sprayer(高地隙喷雾机主动空气悬架减振控制与实验), *Transactions of the Chinese Society for Agricultural Machinery*, vol.49, pp.60-67;
[36] Zirkohi M.M., Lin T.C., (2014), Interval type-2 fuzzy-neural network indirect adaptive sliding mode control for an active suspension system, *Nonlinear Dynamics*, vol.79, pp.513-526.